COLLEGE MATHSTIC
DOCTORAL BRETAGNE
BRETAGNE OCEANE

Université Bretagne Sud

THÈSE DE DOCTORAT DE

L'UNIVERSITÉ DE BRETAGNE SUD

ÉCOLE DOCTORALE N° 644
Mathématiques et Sciences et Technologies de l'Information et de la Communication en Bretagne Océane
Spécialité : *Informatique et Architectures Numériques*

Par
William PENSEC

Protection d'un processeur avec DIFT contre des attaques physiques

« Sous-titre de la thèse »

Thèse présentée et soutenue à Lorient, le //2024
Unité de recherche : Université Bretagne Sud, UMR CNRS 6285, Lab-STICC
Thèse N° : « si pertinent »

Rapporteurs avant soutenance :

Prénom NOM Fonction et établissement d'exercice
Prénom NOM Fonction et établissement d'exercice
Prénom NOM Fonction et établissement d'exercice

Composition du Jury :

Attention, en cas d'absence d'un des membres du Jury le jour de la soutenance, la composition du jury doit être revue pour s'assurer qu'elle est conforme et devra être répercutée sur la couverture de thèse

Président :	Prénom NOM	Fonction et établissement d'exercice *(à préciser après la soutenance)*
Examinateurs :	Prénom NOM	Fonction et établissement d'exercice
	Prénom NOM	Fonction et établissement d'exercice
	Prénom NOM	Fonction et établissement d'exercice
	Prénom NOM	Fonction et établissement d'exercice
Dir. de thèse :	Guy GOGNIAT	Professeur des Universités (Lab-STICC, Université Bretagne Sud)
Co-dir. de thèse :	Vianney LAPÔTRE	Maitre de Conférence HDR (Lab-STICC, Université Bretagne Sud)

Invité(s) :

Prénom NOM Fonction et établissement d'exercice

$\mathcal{A}$d mentes inquisitivas quae lucem futuri Scientiae accendunt.

Aux esprits curieux qui illuminent l'avenir de la Connaissance.

To the inquisitive minds that are lighting up the future of Knowledge.

Remerciements

Je tiens à remercier
I would like to thank. my parents..
J'adresse également toute ma reconnaissance à ....
....

Table of Contents

Acronyms

CABA Cycle Accurate and Bit Accurate

CSR Control and Status Registers

DIFT Dynamic Information Flow Tracking

FIA Fault Injection Attack

ISA Instruction Set Architecture

PC Program Counter

RA Return Address

TCR Tag Check Register

TPR Tag Propagation Register

List of Figures

List of Tables

List of Listings

Chapter 1

Introduction

IoT without security means Internet of Threats

Stéphane Nappo

Contents

1.1 Context

1.2 Motivations

1.3 Objectives

1.4 Manuscript outline

This work is segmented in seven chapters, the first being this introduction.

Chapter 2

Chapter 3 presents the background of this work with the presentation of the RISC-V ISA, the architecture of the D-RI5CY core and the DIFT works. Then, the use cases used in this work are going to be presented. Finally, a vulnerability assessment will be done to show how these use case are vulnerable against FIA and where.

Chapter 4 introduces a new tool to automatise fault injection campaigns in simulation. This tool, FISSA, allows a designer to assess his design during the conception phase. This chapter will present how it works and how to use it, and compares it to others tool available in the literature.

Chapter 5 details the different implementation of countermeasures to protect the D-RI5CY core against FIA and evaluate these protections in terms of area, performance, and efficiency.

Chapter 6

Chapter 7

Chapter 2

State of the Art

Contents

2.1 Introduction

This chapter provides an overview of related work to contextualize the primary objectives of this thesis. Firstly, Information Flow Tracking (IFT) is introduced, detailing the different types and their respective purposes. We will discuss the various levels of monitoring, from program behaviour to the detection of hardware trojans. Subsequently, Physical Attacks are examined, focusing on two main types: Side-Channel Attacks (SCA) and Fault Injection Attacks (FIA). Finally, as this work will concentrate on FIA, we will exclusively present countermeasures against Fault Injection Attacks.

2.2 Information Flow Tracking

This section presents the various types of IFT and the different functional levels associated with Dynamic IFT.

2.2.1 Different types of IFT

There are two distinct types of IFT approaches: static and dynamic, each with its own specific objectives.

2.2.1.1 Static IFT (SIFT)

This approach involves analysing the flow of information within a system without actually executing the program. The goal of static IFT is to determine potential information flows and data pathways by

examining the codebase or system architecture. This method is particularly useful for identifying theoretical vulnerabilities and ensuring compliance with design principles before deployment. Static analysis is comprehensive as it covers all possible execution paths, but it may also generate false positives by flagging theoretical flows that might not occur in practice.

2.2.1.2 Dynamic IFT (DIFT)

In contrast, dynamic IFT tracks information flow in real-time as the system operates. This method observes how data actually moves through the system under various operating conditions, providing a practical and immediate understanding of information handling and leakage. The goal of dynamic IFT is to detect and respond to security breaches or compliance issues as they happen, offering a real-world perspective on the system's security posture. However, this approach might not cover all potential data paths as it is dependent on the specific conditions and inputs provided during the monitoring period.

2.2.2 Different levels of IFT

2.2.2.1 Application level

2.2.2.2 OS level

2.2.2.3 Architecture level

2.2.2.4 Gate level

2.2.3 DIFT Architectures

2.2.3.1 Off-Core

2.2.3.2 Off-Loading

2.2.3.3 In-Core

2.3 Physical Attacks

2.3.1 Side-Channel Attacks

2.3.2 Fault Injection Attacks

2.4 Countermeasures against FIA

Chapter 3

D-RI5CY - Vulnerabilities Assessment

Contents

This chapter provides the background of this thesis and the vulnerability assessment. The first section offers a description of the RISC-V Instruction Set Architecture (ISA) and an overview of the specific RISC-V DIFT design under consideration. The second section details and describes the considered uses cases of this thesis. Finally, the third section assesses the vulnerabilities of the D-RI5CY, using these three cases.

3.1 D-RI5CY

In this section, we describe the RISC-V ISA and detail the DIFT design we have chosen to focus on.

3.1.1 RISC-V Instruction Set Architecture (ISA)

RISC-V is an open and free ISA, which was originally developed at University of California, Berkeley, in 2010, and now is managed and supported by the RISC-V Foundation, having more than 70 members including companies such as Google, AMD, Intel, etc. The architecture was designed with a focus on

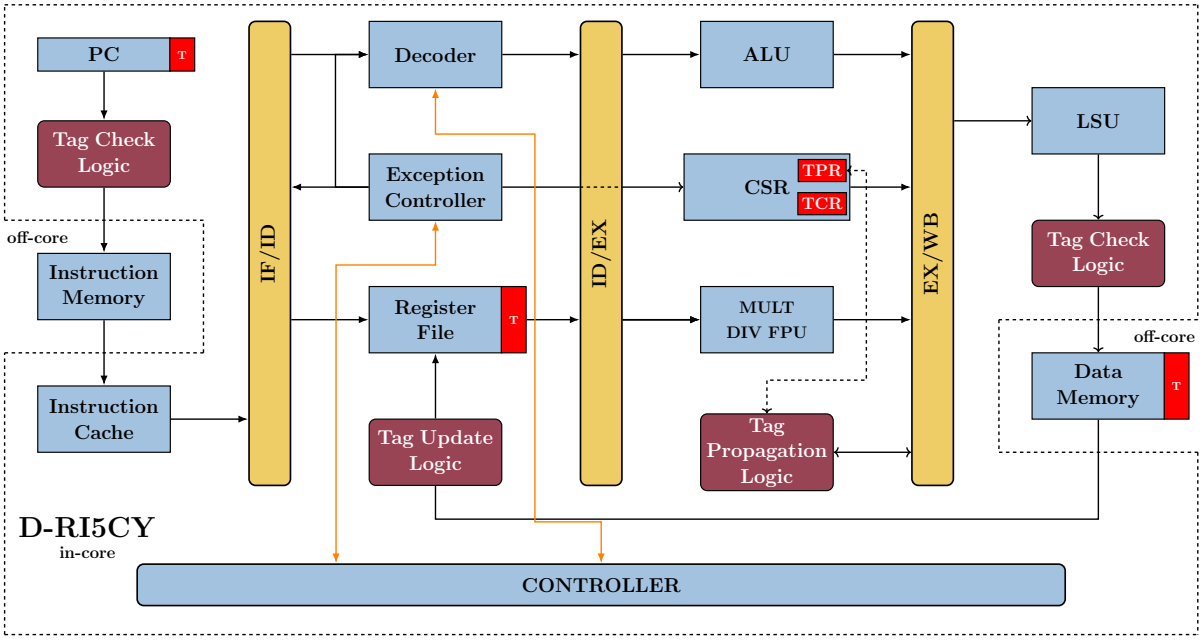

Figure 3.1: D-RI5CY processor architecture overview. DIFT-related modules are highlighted in red.

simplicity and efficiency, embodying the Reduced Instruction Set Computer (RISC) principles. Unlike proprietary ISA, RISC-V is freely available for anyone to use without licensing fees, making it a popular choice for academic research, commercial products, and educational purposes.

Technically, RISC-V features a modular design, allowing developers to incorporate only the necessary components for their specific application, which can significantly reduce the processor's complexity and power consumption. It supports several base integer sets classified by width—mainly RV32I, RV64I, and RV128I for 32-bit, 64-bit, and 128-bit architectures respectively. Each base set can be extended with additional modules for applications requiring floating-point computations (e.g., RV32F, RV64F), atomic operations (e.g., RV32A, RV64A), and more. This modularity and the openness of RISC-V have spurred a wide range of innovations in processor design and applications in areas ranging from embedded systems to high-performance computing.

3.1.2 DIFT design

For this thesis, we opted not to develop a Dynamic Information Flow Tracking (DIFT) system from the ground up, as this would have required considerable time for implementation and testing, which was not within the scope of our objectives. Consequently, we decided to review the current state of the art and select an open-source DIFT system. As a result, we have selected the D-RI5CY [1], [2] design, which utilises the RI5CY core supported by PULPino and developed by ETH Zurich. This is a 4-stage, in-order, 32-bit RISC-V core optimised for low-power embedded systems and IoT applications. It fully supports the base integer instruction set (RV32I), compressed instructions (RV32C), and the multiplication instruction set extension (RV32M) of the RISC-V ISA. Additionally, it includes a set of custom extensions (RV32XPulp) that support hardware loops, post-incrementing load and store instructions, and, ALU and

MAC operations.

D-RI5CY has been developed by researchers of Columbia University, in the USA, in partnership with Politecnico di Torino, in Italy. D-RI5CY use the RI5CY processor, in which they implemented a hardware in-core DIFT.

Figure 3.1 presents an overview of the D-RI5CY processor's architecture. In red and dark red are represented the DIFT specific modules. These modules allow tags to be initialised, propagated and checked during the execution of a sensitive application. The *Tag Update Logic* module is used to initialize or update the tag in the register file according to the tagged data. Then, when a tag is propagated in the pipeline in parallel to its associated data, the *Tag Propagation Logic* module propagates it according to the security policy defined in the *TPR*. Once a tag has been propagated and its data has been sent out of the pipeline, the *Tag Check Logic* modules check that it conforms to the security policy defined in the TCR. If not, an exception is raised and the application is stopped to avoid accessing or executing corrupted data.

The authors of the D-RI5CY defined a library of routines to initialise the tags of the data coming from potentially malicious channels. At program startup, D-RI5CY initialises the tags of the registers, program counter and memory blocks to *zero*. The default 1-bit tag is "*0*", this means that the data is trusted, otherwise, the tag would be set to "*1*" which means that the data is untrusted. They extended the RI5CY ISA with memory and register tagging instructions. They have added four assembly instructions to initialise tags for user-supplied inputs:

- **p.set rd**: sets to untrusted the security tag of the destination register *rd* (you can check the register names in the ISA specification[1] at page 85),
- **p.spsb x0, offset(rt)**: sets to untrusted the security tag of the memory byte at the address of the value stored in *rt + offset*,
- **p.spsh x0, offset(rt)**: sets to untrusted the security tag of the memory half-word at the address of the value stored in *rt + offset*,
- **p.spsw x0, offset(rt)**: sets to untrusted the security tag of the memory word at the address of the value stored in *rt + offset*.

Moreover, they augmented the program counter with a tag of one bit and the register file with one tag per register's byte (marked as T in Figure 3.1). Finally, they added 4-bit tags to the data memory. Each data element is physically stored in memory with its associated tag.

It is worth noting that the D-RI5CY designers have chosen to rely on the *illegal instruction exception* already implemented in the original RI5CY processor to manage the DIFT exceptions. This choice minimizes the area overhead of the proposed solution.

In the Control and Status Registers (CSR), they added two additional 32-bits registers : Tag Propagation Register (TPR) and Tag Check Register (TCR). These registers are used to store the security policy for both tag propagation and tag check. These registers contain a default policy, and they can be modified during runtime with a simple *csr write* instruction, such as `csrw csr, rs1`. These policies consist of rules, which have fine-grain control over tag propagation and tag check for different classes

1. `https://www2.eecs.berkeley.edu/Pubs/TechRpts/2014/EECS-2014-54.pdf`

Table 3.1: Instructions per category

Class	Instructions
Load/Store	*LW, LH[U], LB[U], SW, SH, SB, LUI, AUIPC, XPulp Load/Store*
Logical	*AND, ANDI, OR, ORI, XOR, XORI*
Comparison	*SLTI, SLT*
Shift	*SLL, SLLI, SRL, SRLI, SRA, SRAI*
Jump	*JAL, JALR*
Branch	*BEQ, BNE, BLT[U], BGE[U]*
Integer Arithmetic	*ADD, ADDI, SUB, MUL, MULH[U], MULHSU, DIV[U], REM[U]*

Table 3.2: Tag Propagation Register configuration

	Load/Store Enable	Load/Store Mode	Logical Mode	Comparison Mode	Shift Mode	Jump Mode	Branch Mode	Arith Mode
Bit index	17 16 15	13 12	11 10	9 8	7 6	5 4	3 2	1 0
Policy 1	0 0 1	1 0	1 0	0 0	1 0	1 0	0 0	1 0
Policy 2	1 1 1	1 0	1 0	1 0	1 0	1 0	1 0	1 0

of instructions. The rules specify how the tags of the instruction operands are combined and checked. Table 3.1 shows the different instructions for each category represented in both TPR and TCR.

Table 3.2 shows the TPR configurations for the security policies considered in our work. Each instruction type has a user-configurable 2-bit tag propagation policy field, except for *Load/Store Enable* which has a 3-bit tag. The tag propagation policy determines how the instruction result tag is generated according to the instruction operand tags. For 2-bit fields, value '00' disables the tag propagation and the output tag keeps its previous value, value '01' stands for a logic AND on the 2 operand tags, value '10' stands for a logic OR on the 2 operand tags and value '11' sets the output tag to zero. The *Load/Store Enable* field provides a finer-granularity rule to enable/disable the input operands before applying the propagation rule specified in the *Load/Store Mode* field. This extra tag propagation policy is defined through 3 bits. These bits allow enabling the source, source-address, and destination-address tags, respectively.

Table 3.3 shows the TCR configurations considered in our work. Each instruction type has a user-configurable 3-bits tag control policy field, except for *Execute Check*, *Branch Check* and *Load/Store Check* which have 1, 2 and 4-bits tag control policy fields respectively. The tag control policy determines whether the integrity of the system is corrupted based on the tags of the instruction's operands. The default 3-bits field should be read as follows: the right bit corresponds to input operand 1, the middle bit corresponds to input operand 2 and the left bit corresponds to the output tag of the operation. For each bit set, the corresponding tag is checked to determine whether an exception must be raised. The *Execute Check* field is used to check the integrity of the PC. The *Branch Check* field is used to check both inputs during branch instructions. The right bit is used for input operand 1 and the left bit is used for input operand 2. Finally, the *Load/Store Check* field is used to enable/disable source or destination tags checking during a *load* or *store* instruction. These bits enable or disable the checking of the source tag, source address tag, destination tag and destination address tag.

To summarise, at first ①, D-RI5CY initialises the configuration registers (TPR and TCR) from the default security policy. Then at program startup ②, D-RI5CY initialises all the tags to *trusted* (i.e, set

Table 3.3: Tag Check Register configuration

	Execute Check	Load/Store Check	Logical Check	Comparison Check	Shift Check	Jump Check	Branch Check	Arith Check
Bit index	21	20 19 18 17	16 15 14	13 12 11	10 9 8	7 6 5	4 3	2 1 0
Policy 1	1	1 0 1 0	0 0 0	0 0 0	0 0 0	0 0 0	0 0	0 0 0
Policy 2	0	0 0 0 0	0 0 0	0 0 0	0 0 0	0 0 0	0 0	0 1 1

to 0). The tag propagation ③ and verification ④ happen in the D-RI5CY pipeline in parallel with the standard behaviour, without incurring any latency overhead.

3.1.3 Pedagogical case study

To present the use of the D-RISCY, we will introduce a use case to demonstrate how to use a new security policy and how the DIFT will detect the violation of different security policies. This use case has been developed for pedagogical purposes but does not involve a real software attack.

Listing 3.1 shows the C code used for this use case. Lines 2 to 4 initialize variables, lines 5 and 6 configure a security policy by writing in the TPR and TCR registers thanks to an assembly line. Line 7 tags the variable "`a`" as untrusted (tag is set to "*1*"). In line 8, variables "`a`" and "`b`" are compared to determine which arithmetic operation should be performed. Lines 9 to 21 detail the assembly code generated from the line 8 C statement. It executes the operations according to the values of "`a`" and "`b`" stored in the registers "`a4`" and "`a5`". The "`(a>b)`" condition and its associated branch is computed in line 9, the "`(a-b)`" subtraction in line 14 and the "`a+b`" addition in line 20.

The assembly line in C is constructed from key words *asm volatile*. The template for this assembly line is: "*asm asm-qualifiers (AssemblerTemplate : OutputOperands [: InputOperands [: Clobbers]])*". So to explain briefly, line 7 in Listing 3.1 is composed of a custom assembly instruction "`p.spsw`", that takes the "`x0`" register as target and specifies an address mode using the placeholder "`0(%0)`". Finally, "*:: "r" (&a)*" part specifies the input operand, with "`r`" indicating that a general-purpose register should be used to hold the address of the variable "`a`".

In terms of security policy, depending on which one we use in Table 3.2 and Table 3.3, we will have different results of exception. Security policy 1 propagates the tags with an *OR* logic for five modes (arithmetic, jump, shift, logical, and load/store mode) and enables the propagation of the tag from the source of a load/store. Security policy 1 checks the tags only for the execute check (i.e., PC instruction) and for the source address and destination address for a load/store instruction. In comparison, security policy 2 enables the propagation for all tags and checks tags only for both inputs of arithmetic instructions. To summarise from our application case, if we use security policy 1, the DIFT will detect the *load* instruction before executing the "`a > b`" comparison and raise an exception; whereas if we use security policy 2, the DIFT protection raises an exception when executing the instruction `add a5,a4,a5` (i.e., the "`a+b`" C statement), since variable `a` is untrusted and `b > a`.

In the continuation of this work, this use case will be referred to as *Compare/Compute* and will be utilised as the third case, implementing security policy 2 from Table 3.2 and Table 3.3. The two other use cases will be presented in the following section 3.2.

Listing 3.1: Compare/Compute C Code

```
1   int main(){
2       int a, b = 5, c;
3       register int reg asm("x9");
4       a = reg;
5       asm volatile("csrw 0x700, tprValue");
6       asm volatile("csrw 0x701, tcrValue");
7       asm volatile("p.spsw x0, 0(\%0);" :: "r" (&a));
8       c = (a > b) ? (a-b) : (a+b);
9           //42c:   ble a4,a5,448
10          //430:   addi a5,s0,-16
11          //434:   lw a4,-12(a5)
12          //438:   addi a3,s0,-16
13          //43c:   lw a5,-4(a3)
14          //440:   sub a5,a4,a5
15          //444:   j 45c
16          //448:   addi a5,s0,-16
17          //44c:   lw a4,-12(a5)
18          //450:   addi a3,s0,-16
19          //454:   lw a5,-4(a3)
20          //458:   add a5,a4,a5
21          //45c:   sw a5,-24(s0)
22      return EXIT_SUCCESS;
23  }
```

3.2 Use cases

This section details the considered use cases in our work. The first two use cases come from the original paper [1]. The third use case is a home-made case which is used to analyse the different DIFT part not studied in others use cases.

3.2.1 First use case: Buffer Overflow

The first use case involves exploiting a buffer overflow, potentially leading to a Return-Oriented Programming (ROP) attack[2] and the execution of a shellcode. The attacker exploits the buffer overflow to access the return address (*RA*) register. When the function returns, the corrupted *RA* register is loaded into the *PC* via a *jalr* instruction. This hijacks the execution flow, causing the first shellcode instruction to be fetched from address (*0x6fc*). Due to the DIFT mechanism, the tag associated with the buffer data overwrites the *RA* register tag. As the buffer data is user-manipulated, it is tagged as *untrusted* (tag value = 1). Consequently, when the first shellcode instruction is fetched, the tag associated with the *PC* propagates through the pipeline until the DIFT mechanism detects a violation of the security policy and raises an exception. This attack demonstrates the behaviour of DIFT when monitoring the *PC* tag. This use case employs the first security policy from Table 3.2 and Table 3.3.

To illustrate the use of TCR and TPR registers, we assume that buffer data tags are set to 1 (i.e., *untrusted*) since the user manipulates the buffer. To detect this kind of attack, it is necessary to ensure the PC integrity by prohibiting the use of untrusted data for this register (i.e., *Execute Check* field of TCR set to 1). Regarding tag propagation configuration, load, and store input operand tags must be propagated to output. Thus, the TPR register *Load/Store Mode* field should be set to value 10 (i.e. destination tag = source tag) and the *Load/Store Enable* field must be set to 001 (i.e., Source tag enabled).

Listing 3.2 displays the C code for the buffer overflow scenario. The assembly code on line 22 of this listing represents the saving of the register *x8*, which is the *saved register 0* or *frame pointer* register in the RISC-V ISA. Next, the source buffer is filled with A's characters and the shellcode address is appended to the end of this source buffer. Finally, lines 30-33 illustrate the tag initialisation on the source buffer.

2. `https://github.com/sld-columbia/riscv-dift/blob/master/pulpino_apps_dift/wilander_testbed/`

Figure 3.2 represents the five steps from the source buffer initialisation to the first shellcode instruction being fetched. In Figure 3.2a, the source buffer, in yellow, is initialised with A's, and as it is manipulated by a user, it is tagged as untrusted (red). The destination buffer is empty, and both *PC* and *RA* register are trusted (green). In Figure 3.2b, the source buffer is copied into the destination buffer, the data and the tag are copied. In Figure 3.2c, the overflow occurs and the *ra* register is compromised with the address of the shellcode function from the source buffer. Now, all the memory tags are untrusted. In Figure 3.2d, the *PC* loads the *ra* register along with its tag. The *PC* loses its integrity and became untrusted. In Figure 3.2e, the *PC* address is fetched, and the instruction is sent into the pipeline along with the tag. At this moment, the DIFT mechanism will detect the untrusted tag and as the security policy do not allow executing an untrusted PC, an exception will be raised and the application will be stopped.

Listing 3.2: Buffer overflow C code

```
1  #define BUFSIZE 16
2  #define OVERFLOWSIZE 256
3
4  int base_pointer_offset;
5  long overflow_buffer[OVERFLOWSIZE];
6
7  int shellcode() {
8      printf("Success !!\n");
9      exit(0);
10 }
11
12 void vuln_stack_return_addr(){
13     long *stack_pointer;
14     long stack_buffer[BUFSIZE];
15     char propolice_dummy[10];
16     int overflow;
17
18     /* Just a dummy pointer setup */
19     stack_pointer = &stack_buffer[1];
20
21     /* Store in i the address of the stack frame section dedicated to function arguments */
22     register int i asm("x8");
23
24     /* First set up overflow_buffer with 'A's and a new return address */
25     overflow = (int)((long)i - (long)&stack_buffer);
26     memset(overflow_buffer, 'A', overflow-4);
27     overflow_buffer[overflow/4-1] = (long)&shellcode;
28
29     /* TAG INITIALISATION */
30     for(int j=0; j<overflow/4; j++) {
31         asm volatile ("p.spsw x0, 0(%[ovf]);"
32                       ::[ovf] "r" (overflow_buffer+j));
33     }
34
35     /* Then overflow stack_buffer with overflow_buffer */
36     memcpy(stack_buffer, overflow_buffer, overflow);
37
38     return;
39 }
40
41 int main(){
42     vuln_stack_return_addr();
43     printf("Attack prevented.\n");
44     return EXIT_SUCCESS;
45 }
```

3.2.2 Second use case: Format String (WU-FTPd)

The second use case is a format string attack[3] overwriting the return address of a function to jump to a shellcode and starts its execution. This use case uses the first security policy from Table 3.2 and Table 3.3. This attack exploits the `printf()` function from the C library. It uses the `%u` and `%n` formats (see Chapter 12, Section 12.14.3 in [3] for detailed information) to write the targeted address.

Listing 3.3 shows the C code of this use case. The `echo` function assign the *x8* register to a variable '`i`' which goes into another variable '`a`'. The lines 13-14 are used to initialise the tag associated to the

3. `https://github.com/sld-columbia/riscv-dift/tree/master/pulpino_apps_dift/wu-ftpd`

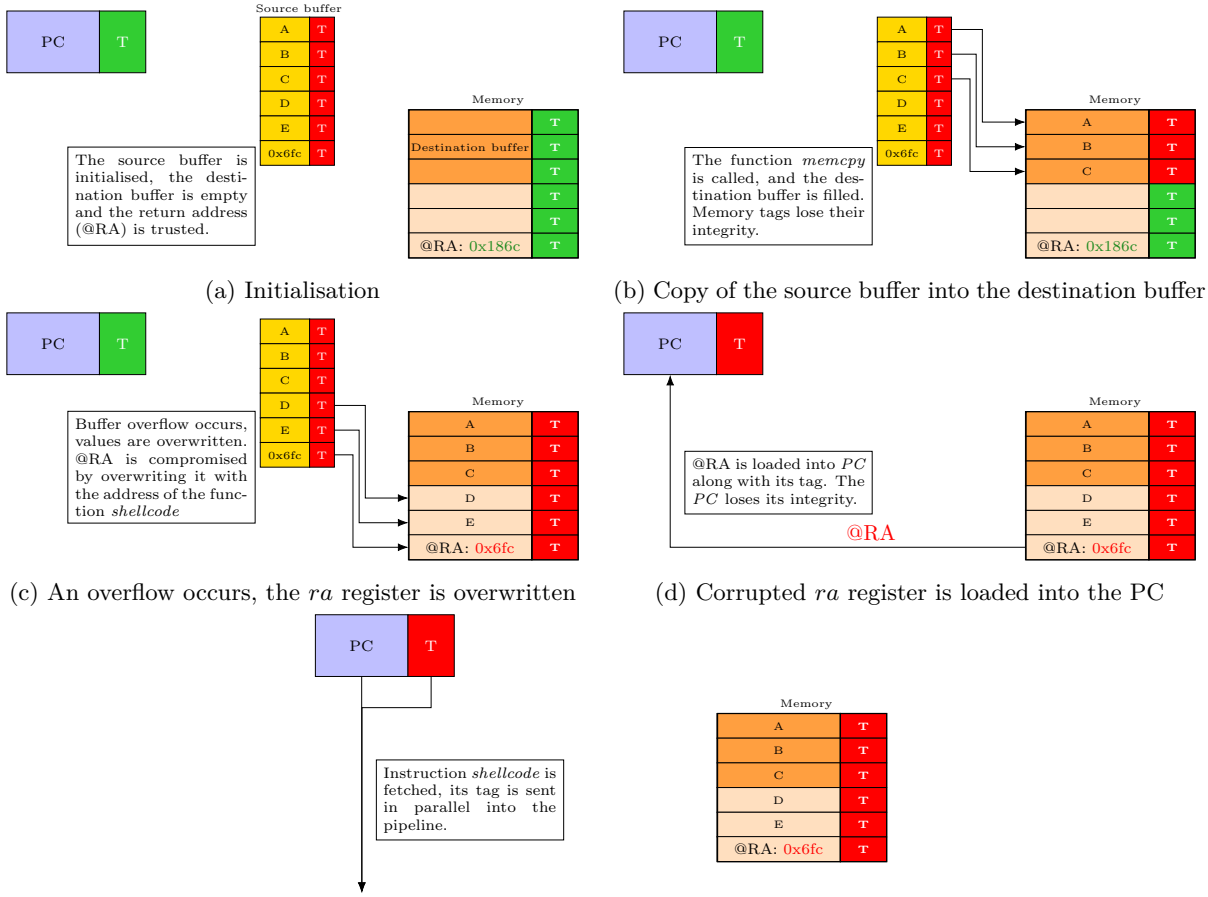

(a) Initialisation

(b) Copy of the source buffer into the destination buffer

(c) An overflow occurs, the *ra* register is overwritten

(d) Corrupted *ra* register is loaded into the PC

(e) PC address instruction is fetched

Figure 3.2: Representation of how the ROP attack works

variable 'a'. This variable 'a' is user-defined, so it is tagged as untrusted for DIFT computation. The vulnerable statement is the `printf` statement in line 16. The format `%u` is used to print unsigned integer characters. The format `%n` is used to store in memory the number of characters printed by the `printf()` function, the argument it takes is a pointer to a signed int value.

The execution of the `printf` at line 16 leads to write in memory 224 (0xe0) at address (a-4), 224+35 so 259 (0x103) at address (a-3), and 512 (0x200) at addresses (a-2) and (a-1). The attacker's objective is to overwrite the return address with '*0x3e0*' which represent the address of the first function, called *secretFunction* in Listing 3.3. In this case, security policy prohibits the use of untrusted variables as store addresses. Since variable 'a' is untrusted, the DIFT protection raises an exception when storing a value at memory address `(a-4)`. This use case has been chosen to activate the load/store modes of the DIFT policy.

Table 3.4 represents the different steps to overwrite the memory with the exact address of the malicious function. We can see that after each write and the right shift of the writing, the address appears. Finally, we have the address '*000002000003E0*' in memory from 'A+2' to 'A-4' but as an address is on 32-bits in

Listing 3.3: WU-FTPd C code

```
void secretFunction(){
    printf("Congratulations!\n");
    printf("You have entered in the secret function!\n");

    exit(0);
}

void echo(){
    int a;
    register int i asm("x8");
    a = i;

    asm volatile ("p.spsw x0, 0(%[a]);"
                  ::[a] "r" (&a));

    printf("%224u%n%35u%n%253u%n%n", 1, (int*) (a-4), 1, (int*) (a-3), 1, (int*) (a-2), (int*) (a-1));

    return;
}

int main(int argc, char* argv[]){
    volatile int a = 1;

    if(a)
        echo();
    else
        secretFunction();

    return 0;
}
```

Table 3.4: Memory overwrite

Address	A-4	A-3	A-2	A-1	A	A+1	A+2
A-4	*0xE0*	*0x00*	*0x00*	*0x00*			
A-3		*0x03*	*0x01*	*0x00*	*0x00*		
A-2			*0x00*	*0x02*	*0x00*	*0x00*	
A-1				*0x00*	*0x02*	*0x00*	*0x00*
Memory	0xE0	0x03	0x00	0x00	0x02	0x00	0x00

our architecture, the address fetched by the pipeline is only '*000003E0*'.

3.3 Vulnerability assessment

In order to analyse the behaviour of the processor at application runtime against Fault Injection Attacks, we have simulated some fault injections campaigns in which we inject fault inside the 55 registers associated to the DIFT, which correspond to 127 bits in total. For these campaigns, we use a tool, developed for this purpose. This tool is described in Chapter 4 and can generate the TCL code to automatise fault injections attacks campaigns at Cycle Accurate and Bit Accurate (CABA) level. Table 3.5 shows the repartition of these registers in every pipeline stage of the RI5CY core and the number of associated bits. This work has been published in ACM Sensors S&P [4].

We assess the design with fault injection campaigns. With their results associated, we can deduce which registers are vulnerable with the cycle associated and the fault model. This assessment is done for each use case for a more precise analysis and to understand how the tag is propagated and checked before the exception.

Table 3.5: Numbers of registers and quantity of bits represented

HDL Module	**Number of registers**	**Number of bits in registers**
Instruction Fetch Stage	2	2
Instruction Decode Stage	14	19
Register File Tag	1	32
Execution Stage	1	1
Control and Status Registers	2	64
Load/Store Unit	4	9
Total	**24**	**127**

Table 3.6: Buffer overflow: success per register, fault type and simulation time

	Cycle 3428			Cycle 3429			Cycle 3430			Cycle 3431			Cycle 3432		
	set0	set1	bit-flip	set0	set1	bit-flip	set0	set1	bit-flip	set0	set1	bit-flip	set0	set1	bit-flip
pc_if_o_tag										✓		✓			
rf_reg[1]							✓		✓						
tcr_q	✓			✓			✓			✓			✓		
tcr_q[21]			✓			✓			✓			✓			✓
tpr_q	✓	✓		✓	✓										
tpr_q[12]			✓			✓									
tpr_q[15]			✓			✓									

3.3.1 Fault model for vulnerability assessment

In this vulnerability assessment, we consider an attacker able to inject faults into DIFT-related registers leading to *set to 0*, *set to 1*, and *single bit-flip in one register at a given clock cycle*. To bypass the DIFT mechanism, the main attacker's goal is to prevent an exception being raised. To reach this objective, any DIFT-related register maintaining tag value, driving the tag propagation or the tag update process or maintaining the security policy configuration can be targeted.

3.3.2 First use case: Buffer overflow

Table 3.6 shows that 22 fault injections in four different DIFT-related registers can lead to a successful attack despite the DIFT mechanism (i.e., DIFT protection is bypassed). For example, it shows that a fault injection targeting the *pc_if_o_tag* register can defeat the DIFT protection if a fault is injected at cycle 3431 using a bit-flip or a set to 0 fault type. Furthermore, Table 3.6 shows that five different cycles can be targeted for the attack to succeed. In most cases, *bit-flip* leads to a successful injection with 11 successes over 22. Faults in *tpr_q* and *tcr_q* are successful, since these registers maintain the propagation rules and the security policy configuration (see Table 3.2 and Table 3.3 for more details about each bit position). Both *pc_if_o_tag* and *rf_reg[1]* are also critical registers for this use case. Indeed, *pc_if_o_tag* allows the propagation of the PC tag while *rf_reg[1]* stores the tag of the return address register *ra*.

Now that we have these results, we can analyse them and present an in-depth analysis of the simulation results leading to successful attacks. The aim is to understand why an attack succeeds. For that purpose, we study the propagation of the fault through both temporal and logical views. Most of the faults

targeting both TPR and TCR registers are not detailed in this section. Indeed, these faults mainly target the DIFT configuration and not the tag propagation and tag-checking computations. Faults targeting these registers can be performed in any cycle prior to their use.

Figure 3.3 presents the *ra* register tag propagation in the context of the first use case for a non-faulty execution. It focuses on three clock cycles from the decoding of a `jalr` instruction (i.e., returning from the called function) to the DIFT exception due to a security policy violation. In cycle 3430, this tag is extracted from the *register file tag* (i.e., from *rf_reg[1]*). In cycle 3431, it is propagated to the *pc_if_o_tag* register. Then, in cycle 3432, it is propagated in the *pc_id_o_tag* register and the first shellcode instruction is decoded. Since *ra* is tagged as untrusted and the security policy prohibits the use of tagged data in PC (*Execute Check* bit = 1 in Table 3.3), an exception is raised during the tag check process, which is performed in parallel of the first shellcode instruction decoding.

Figure 3.3 illustrates the reason behind the sensitivity of registers *rf_reg[1]* and *pc_if_o_tag* at cycles 3430, 3431 and 3432 highlighted in Table 3.6. We can note that *pc_id_o_tag* register does not appear in Table 3.6 while Figure 3.3 shows its role during tag propagation. Actually, this register gets its value from *pc_if_o_tag*, so a fault injection in this register only delays the exception.

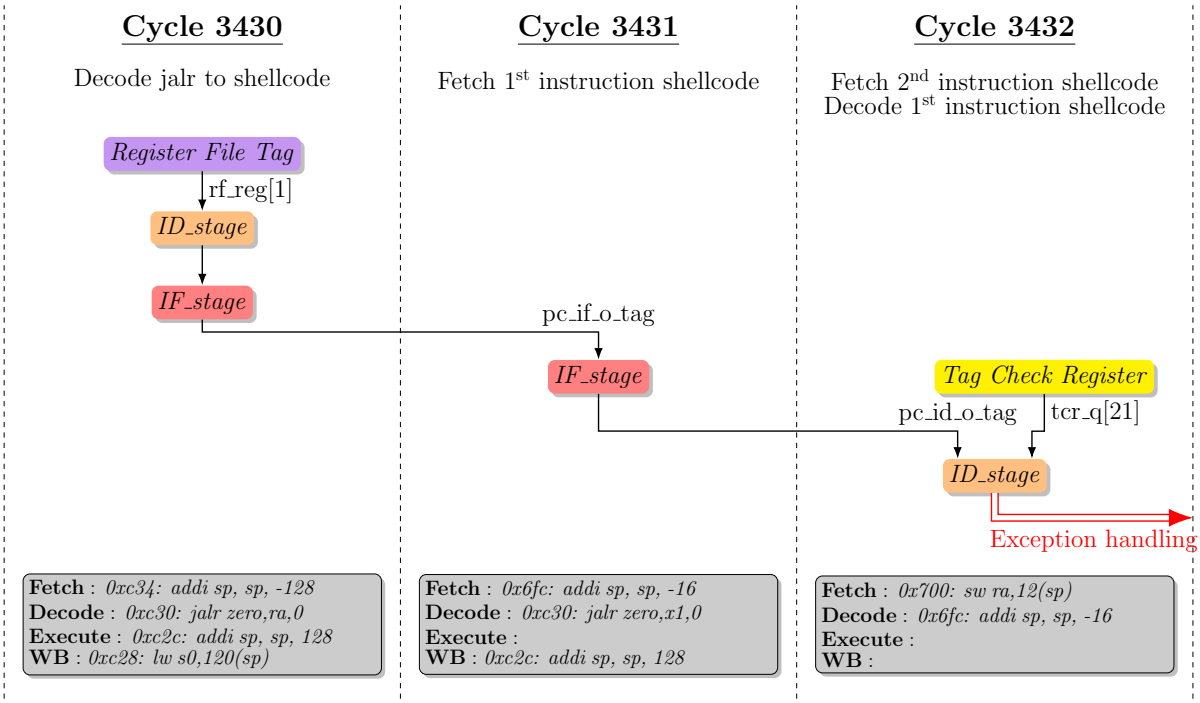

Figure 3.3: Tag propagation in a buffer overflow attack

To further study the propagation of the fault, Figure 3.4 illustrates the logical relations between the DIFT-related registers (yellow boxes) and control signals or processor registers (grey boxes) driving the illegal instruction exception signal (red box). This figure does not describe the actual hardware architecture but highlights the logic path leading to an exception raise. An attacker performing fault injections would like to drive the exception signal to '0' to defeat the D-RI5CY DIFT solution. Figure 3.4 shows that a single fault could lead to a successful injection since all logic paths are built with *AND* gates.

For instance, if register *rf_reg[1]* is set to 0, the tag will be propagated from *gate 1* to *gate 4*. Then, *gate 5* inputs are *tcr_q[21]* (i.e., '1') and *pc_id_o_tag* (i.e., '0', *gate 4* output). Thus, *gate 5* output is driven to '0', disabling the exception. From Figure 3.4, three fault propagation paths can be identified: from *gate 1* to *gate 5* if the fault is injected into *rf_reg[1]*, from *gate 4* to *gate 5* if a fault is injected into *pc_if_o_tag* and through *gate 5* if a fault is injected into either the *tcr_q* or *pc_id_o_tag*. Analysis of Figure 3.4 strengthens the results presented in Table 3.6 where *set to 0* and *bit-flip* fault types lead to successful attacks. The root cause is that the propagation paths consist entirely of *AND* gates.

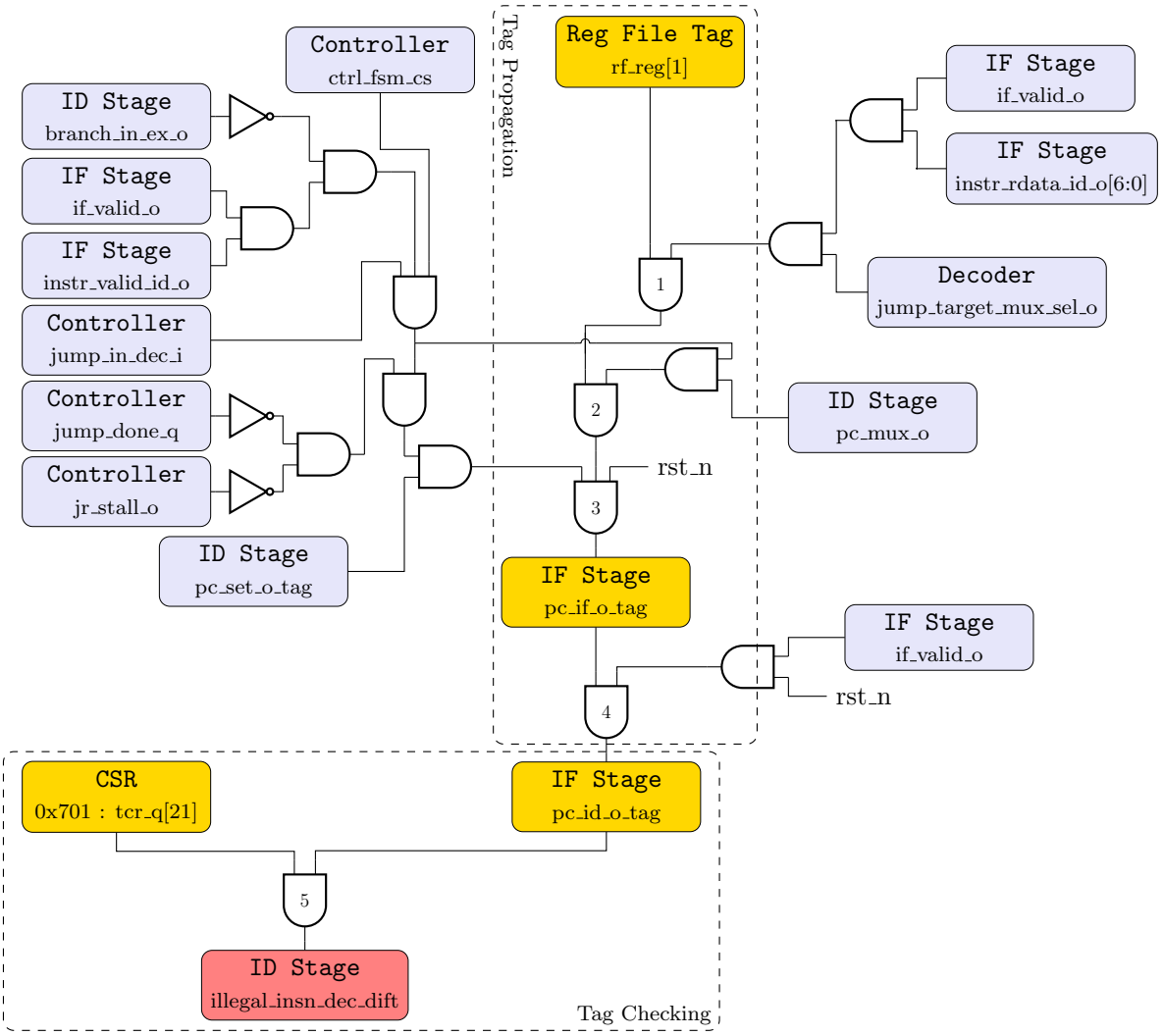

Figure 3.4: Logic description of the exception driving in a buffer overflow attack

3.3.3 Second use case: Format string (WU-FTPd)

Table 3.7 shows that 52 fault injections in 10 DIFT-related registers can lead to a successful attack. Furthermore, it shows that 8 different cycles can be targeted for the attack to succeed. 29 successes over

52 are obtained with the *bit-flip* fault type. *alu_operand_a_ex_o_tag*, *alu_operand_b_ex_o_tag* and *alu_operator_o_mode* registers are critical during cycles 52477 and 52478 since they are used for tag propagation related to the C statement `(a-4)`. *alu_operand_a_ex_o_tag* and *alu_operand_b_ex_o_tag* sequentially store the tag associated to '`a`' while *alu_operator_o_mode* stores the propagation rule according to the TPR configuration (see Table 3.2). *regfile_alu_waddr_ex_o_tag* stores the destination register index in which the tag resulting from tag propagation should be written. *check_s1_o_tag* maintains the TCR value from the decode stage to the execution stage, it is compared to the value of the operand tag for tag checking. *rf_reg[15]* stores the tag associated with the '`a`' variable. *store_dest_addr_ex_o_tag* maintains the tag of the destination address during a store instruction in the execute stage. *use_store_ops_ex_o* drives a multiplexer to propagate the value stored in *store_dest_addr_ex_o_tag* register to the tag checking module. Finally, faults in *tpr_q* and *tcr_q* are successful, since these registers maintain the propagation rules and the security policy configuration. The last two registers, *tpr_q* and *tcr_q* are critical when we fault the bit 12 of TPR because the load/store mode which is set to *10* but if we change it the propagation policy will change and then the tag will not be propagated as a mode set to *11* will clear the tag. A bit-flip at bit 15 will impact the behaviour as it stores the load/store enable source tag. Finally, bit 20 of TCR store the load/store check destination address tag, which is used when the program wants to store at the address (a-4).

Figure 3.5 details the tag propagation in the context of a format string attack case for a non-faulty execution and illustrates the reason behind the sensitivity of registers highlighted in Table 3.7. Figure 3.5 focuses on three clock cycles dedicated to the instruction `sw a4,0(a5)` decoding and execution which should lead to the storage of the value 224 at address (a-4). In cycles 52482 and 52483, `sw a4,0(a5)` is decoded and the source operands tag are retrieved from the tag register file. Particularly, the store destination address is retrieved from *rf_reg[15]* and stored in register *store_dest_addr_ex_o_tag*. In cycle 52484, the destination address of the store operation is computed by the processor Arithmetic Logic Unit (ALU). In parallel, *alu_operator_o_mode*, *alu_operand_a_ex_o_tag*, *alu_operand_b_ex_o_tag*, *store_dest_addr_ex_o_tag* and *check_s1_o_tag* registers drives the tag computation corresponding to the destination address. *use_store_ops_ex_o* drives a multiplexer to propagate the value stored in *alu_operand_a_ex_o_tag* register to the tag checking module. *alu_operand_a_ex_o_tag* and *alu_operand_b_ex_o_tag* sequentially store the tag associated to '`a`' while *alu_operator_o_mode* stores the propagation rule according to the TPR configuration (see Table 3.2). *check_s1_o_tag* maintains the TCR value from the decode stage to the execution stage, it is compared to the value of the operand tag for tag checking. Then, the store should be executed in the Execute stage. However, the tag associated with the store destination address is set to 1 due to tag propagation (since it is computed from variable '`a`'). Since the security policy prohibits the use of data tagged as *untrusted* as a store instruction destination address (*Load/Store Check* field of TCR = 1010), an exception is raised. *use_store_ops_ex_o*, highlighted in Table 3.7 but not shown in Figure 3.5, drives a multiplexer leading to the propagation of register *store_dest_addr_ex_o_tag*.

Table 3.7: Format string attack: success per register, fault type and simulation time

	Cycle 52477			Cycle 52478			Cycle 52479			Cycle 52480			Cycle 52481			Cycle 52482			Cycle 52483			Cycle 52484		
	set0	set1	bit-flip	set0	set1	bit-flip	set0	set1	bit-flip	set0	set1	bit-flip	set0	set1	bit-flip	set0	set1	bit-flip	set0	set1	bit-flip	set0	set1	bit-flip
alu_operand_a_ex_o_tag	✓		✓																					
alu_operand_b_ex_o_tag				✓		✓																		
alu_operator_o_mode	✓	✓		✓	✓																			
alu_operator_o_mode[0]			✓			✓																		
alu_operator_o_mode[1]			✓			✓																		
check_s1_o_tag																						✓		✓
regfile_alu_waddr_ex_o_tag[1]															✓									
rf_reg[15]																✓		✓	✓		✓			
store_dest_addr_ex_o_tag																						✓		✓
tcr_q	✓			✓			✓			✓			✓			✓			✓					
tcr_q[20]			✓			✓		✓			✓				✓			✓			✓			
tpr_q		✓			✓		✓			✓			✓											
tpr_q[12]			✓			✓		✓			✓				✓									
tpr_q[15]			✓			✓		✓			✓				✓									
use_store_ops_ex_o																						✓		✓

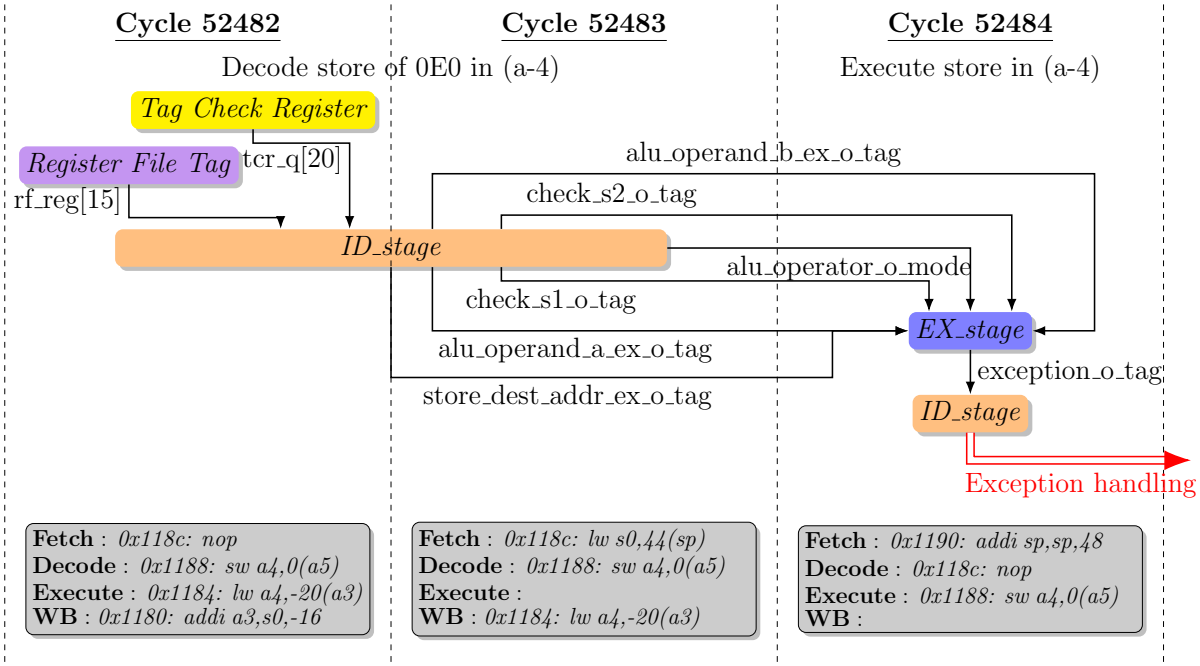

Figure 3.5: Tag propagation in a format string attack

To further study the propagation of the fault, Figure 3.6 illustrates the logical relations between the DIFT-related registers (yellow boxes) and control signals or processor registers (gray boxes) driving the illegal instruction exception signal (red box) for the second use case. Figure 3.6 shows that a single fault could lead to a successful injection, since all logic paths are built with *AND* gates. For instance, if register *rf_reg[15]* is set to 0, this tag value will be propagated from *gate 8* to *gate 11* and to *mux 12*. Then, since *mux 12* output drives one *gate 3* input, *gate 3* output is driven to '0', the exception is disabled. From Figure 3.6, seven fault propagation paths can be identified: from *gate 1* to *gate 3* if the fault is injected into *tcr_q[20]*, through *gate 3* if a fault is injected into *check_s1_o_tag*, from *gate 4* or *gate 5* to *gate 3* if a fault is injected into *alu_operand_b_ex_o_tag* or *alu_operand_a_ex_o_tag*, from *mux 6* to *gate 3* if a fault is injected into *alu_operator_o_mode*, from *mux 7* to *gate 3* if a fault is injected into *regfile_alu_waddr_ex_o_tag*, from *gate 8* to *gate 3* if a fault is injected in the tag register file (i.e., register *rf_reg[15]*) and from *mux 11* to *gate 3* if a fault is injected in either *store_dest_addr_ex_o_tag* or *use_store_ops_ex_o*. Analysis of Figure 3.6 reinforces the results presented in Table 3.7 where *set to 0* and *bit-flip* fault types lead to successful attacks. As with the first use case, the main cause is that the propagation paths are fully made of *AND* gates. As shown in Table 3.7 *alu_operator_o_mode* register is sensitive to *set to 0* and *set to 1* fault types. Indeed, this register determines the tag propagation according to TPR. The tag propagation is disabled when a TPR field is set to '00' and the output tag is set to 0 (i.e., trusted) when a TPR field is set to '11'.

Table 3.8: Compare/compute: number of faults per register, per fault type and per cycle

	Cycle 832			Cycle 833			Cycle 834			Cycle 835		
	set0	set1	bit-flip	set0	set1	bit-flip	set0	set1	bit-flip	set0	set1	bit-flip
alu_operand_a_ex_o_tag										✓		✓
check_s1_o_tag										✓		✓
rf_reg[14]				✓		✓	✓		✓			
tcr_q	✓			✓			✓					
tcr_q[0]			✓			✓			✓			
tpr_q		✓										
tpr_q[12]			✓									
tpr_q[15]			✓									
use_store_ops_ex_o											✓	✓

3.3.4 Third use case: Compare/Compute

Table 3.8 shows that 19 fault injections in 6 DIFT-related registers can lead to a successful attack. Furthermore, it shows that 4 different cycles can be targeted for the attack to succeed. The highest success rate is obtained with the *bit-flip* fault type, with 10 successes over 19. Faults in *rf_reg[14]* and *alu_operand_a_ex_o_tag* are successful, since these registers store the tag associated to variable `a` during tag propagation. *check_s1_o_tag* maintains one configuration bit from *tcr_q* during tag checking. *use_store_ops_ex_o* drives a multiplexer to propagate the value stored in *alu_operand_a_ex_o_tag* register to the tag checking module. For this case, the critical registers can be found in previous case, *alu_operand_a_ex_o_tag* propagate the tag of the tagged variable in the code (variable `a`). Finally, observations for both *tpr_q* and *tcr_q* are similar than for previous case studies. Finally, faults in *tpr_q* and *tcr_q* are successful, since these registers maintain the propagation rules and the security policy configuration.

Figure 3.7 focuses on the three cycles, represented in red, corresponding to `add a5,a4,a5` instruction (C statement `(a+b)`) decoding and execution in the context of the third use case. The instruction `add a5,a4,a5` is in decode stage during cycles 833 and 834 and the tag associated to the untrusted variable `a` is retrieved from *rf_reg[14]*. In cycle 835, this addition is executed. In parallel, variable `a` tag is propagated to the tag check logic unit, which behaviour is driven by *check_s1_o_tag* through *alu_operand_a_ex_o_tag*. Since the V2 security policy prohibits the use of untrusted data as a source operand of an arithmetic operation, an exception is raised.

Figure 3.7 illustrates the reason behind the sensitivity of registers *rf_reg[14]*, *alu_operand_a_ex_o_tag* and *check_s1_o_tag* highlighted in Table 3.8. Note that *use_store_ops_ex_o* does not appear in Figure 3.7. This register drives a multiplexer leading to tag propagation presented in Figure 3.7.

To further study the faults' propagation, Figure 3.8 illustrates the logical relations between the DIFT-related registers (yellow boxes) and control signals or processor registers (gray boxes) driving the illegal instruction exception signal (red box). Figure 3.8 shows that a single fault could lead to a successful injection, since all logic paths are built with *AND* gates. For instance, if register *rf_reg[14]* is set to 0, the tag will be propagated from *gate 8* to *gate 10* and to *mux 12*. Then, since *mux 12* output drives one *gate 3* output, the exception is disabled. From Figure 3.8, seven fault propagation paths can be identified. We won't go into detail here about the seven different paths, as they were mentioned in case 2, bearing in mind that colour differentiation must be taken into account (for example: *alu_operand_a_ex_o_tag*

instead of *store_dest_addr_ex_o_tag* from *gate 1* to *gate 3* if the fault is injected into *tcr_q[0]*, through *gate 3* if a fault is injected into *check_s1_o_tag*, from *gate 4* or *gate 5* to *gate 3* if a fault is injected into *alu_operand_b_ex_o_tag* or *alu_operand_a_ex_o_tag*, from *mux 6* to *gate 3* if a fault is injected into *alu_operator_o_mode*, from *mux 7* to *gate 3* if a fault is injected into *regfile_alu_waddr_ex_o_tag*, from *gate 8* to *gate 3* if a fault is injected into *rf_reg[14]*, and from *mux 11* to *gate 3* if a fault is injected into either *alu_operand_a_ex_o_tag* or *use_store_ops_ex_o*. Analysis of Figure 3.8 supports the results presented in Table 3.8 where *set to 0* and *bit-flip* fault types lead to successful attacks. As with first and second use cases, the main reason is that the propagation paths are built entirely from *AND* gates.

3.4 Summary

In this chapter, we described the processor we focus on with its implementation of a hardware in-core DIFT. We described how it works and how to use the DIFT mechanism with the default configuration. Then, we described the different use cases we choose to work with, in order to analyse the DIFT behaviour and assess it against fault injection attacks. Finally, we presented the vulnerability assessment on these use cases using the D-RI5CY security mechanism. We shown that this DIFT implementation is vulnerable to FIA within different registers depending on the fault model and depending on the application, as different paths are used and so different registers are going to be criticals.

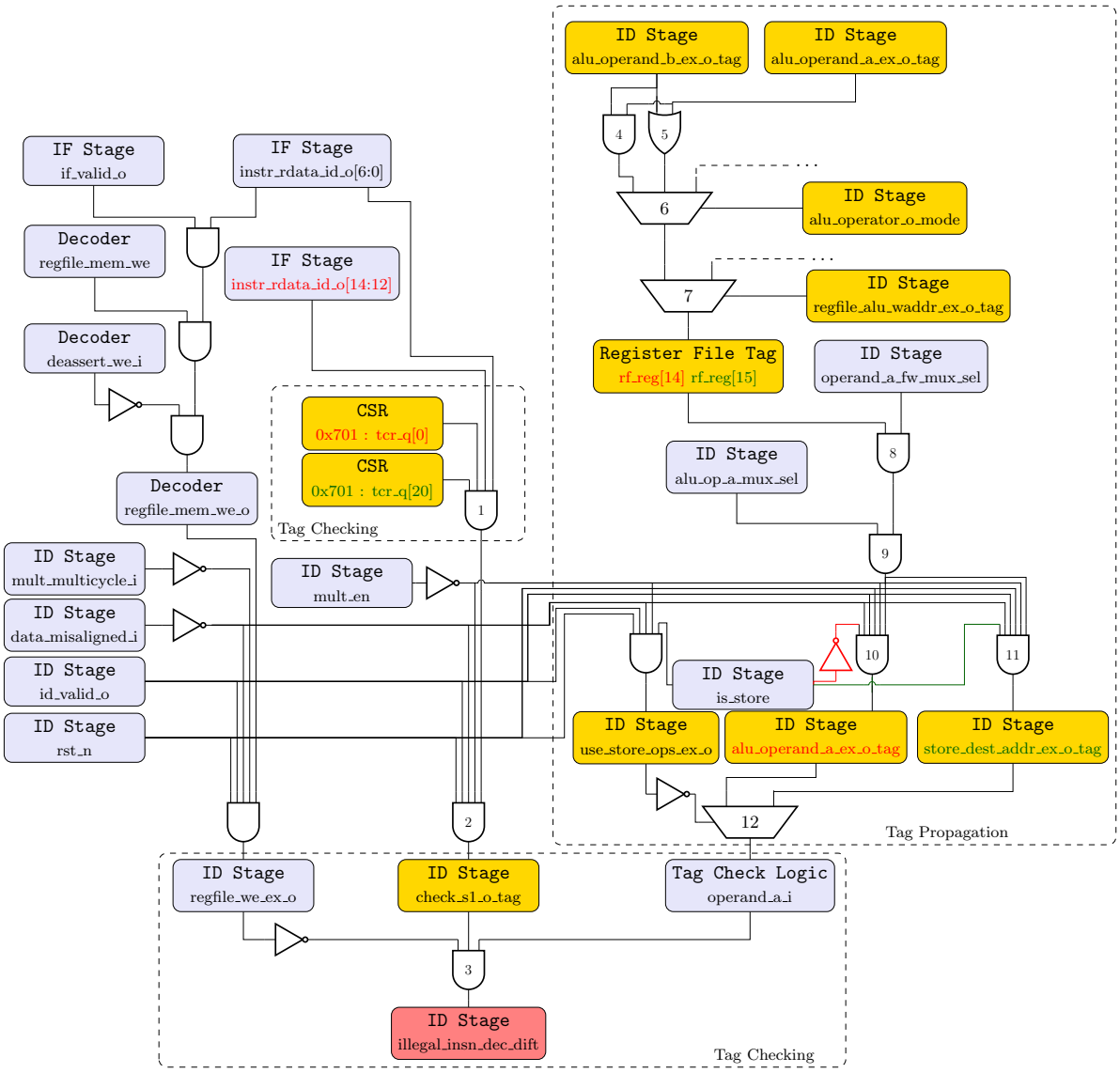

Figure 3.6: Logic description of the exception driving in a format string attack

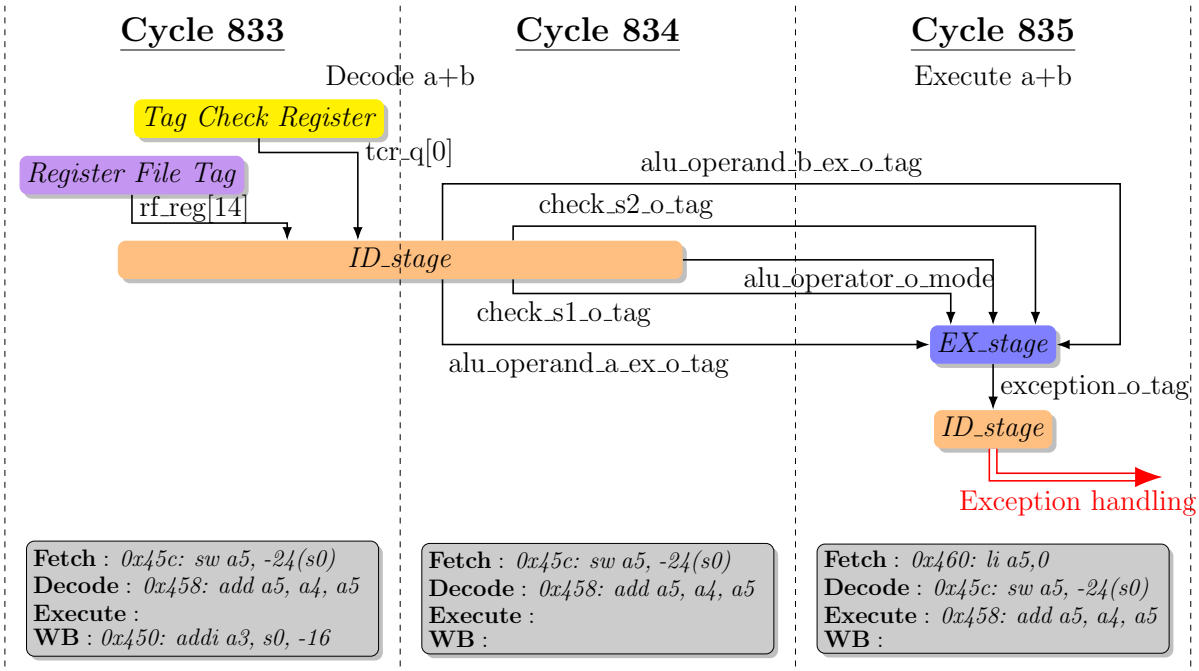

Figure 3.7: Tag propagation in a computation case with the compare/compute use case

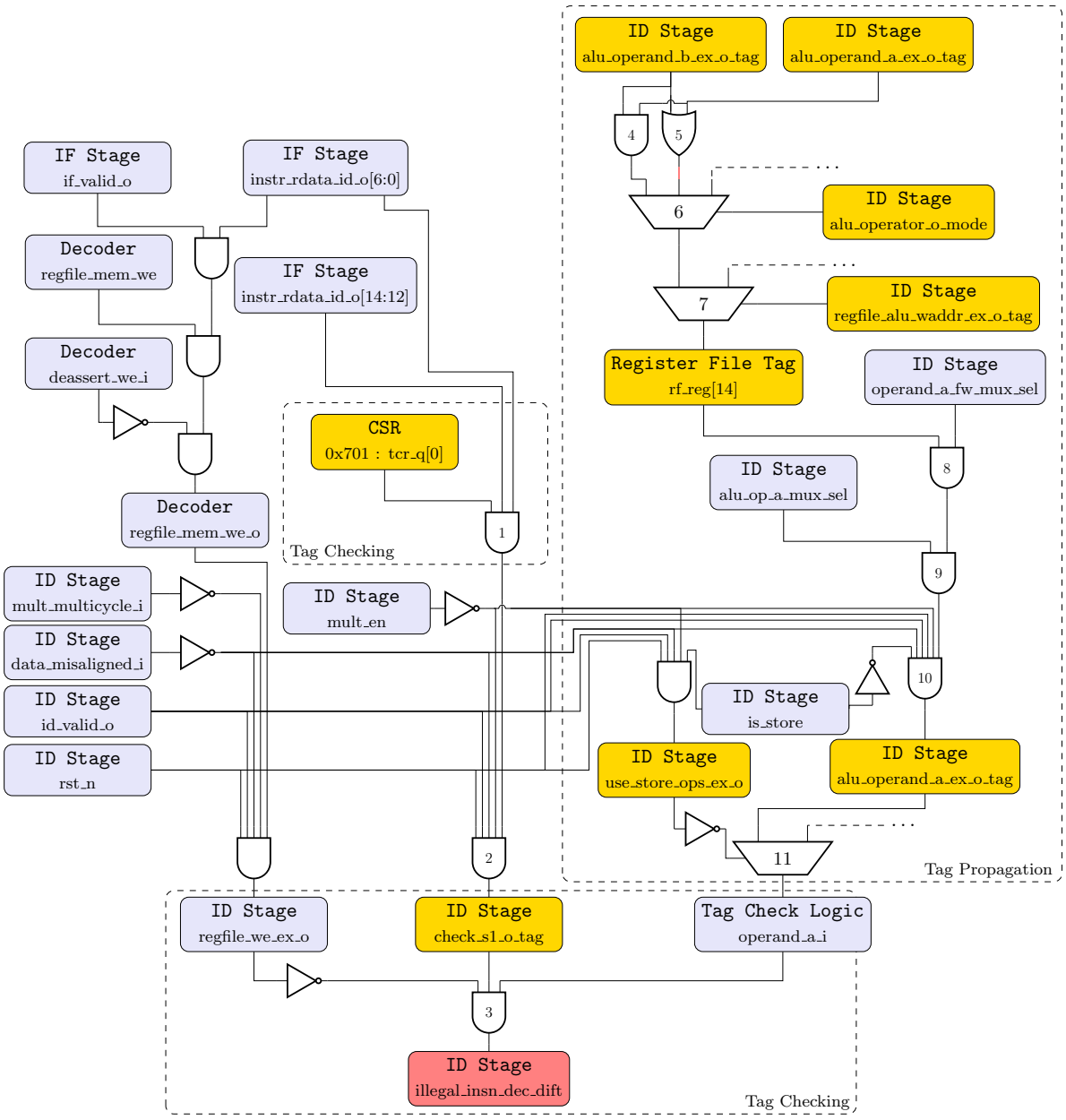

Figure 3.8: Logic representation of tag propagation in a computation case

Chapter 4

FISSA – Fault Injection Simulation for Security Assessment

Contents

This section introduces and presents a tool, called FISSA – Fault Injection Simulation for Security Assessment –, created to automate fault injection attacks campaigns in simulation. The first section presents the state of the art of existing tools for FIA campaigns in emulation, formal methods or even perform real world attacks. The second section presents the architecture and details how FISSA works and presents how to extend it depending on other needs. Finally, we will discuss and draw some perspectives for the tool's development and usability.

4.1 Simulation tools for Fault Injection

This section presents recent works related to methods and tools for vulnerability assessment when considering fault injection attacks. For such vulnerability assessment, main strategies include actual fault injections, emulations, formal methods and simulations.

Actual FIAs involve physically injecting faults into the target hardware using techniques such as variations in supply voltage or clock signal [16], [17], laser pulses [16], [19], electromagnetic emanations [16] or X-Rays [18]. This approach offers valuable insights into the real impact of faults on hardware components.

Table 4.1: Fault Injection based methods for vulnerability assessment comparison

	References	Cost	Control over fault scenarios	Scalability	Speed of execution	Realism	Expertise
Formal Methods	[5]–[8]	Very low	Very high	Very low	Low	Low	Very high
Simulations	[9]–[11]	Very low	Very high	Low	Low/Moderate	Moderate	Low
Emulations	[12]–[15]	High	Moderate	High	Very high	High	Moderate
Actual FIA	[16]–[19]	Very high	Very low	Very high	Very high	Very high	Very high

However, a significant drawback of actual fault injections is that they demand considerable expertise to prepare the target, involving intricate setup procedures. Additionally, this approach can only be executed once the physical circuit is available, potentially delaying the vulnerability assessment process until later stages of development.

Fault emulation can, for instance, rely on FPGA [12], or on an emulator such as QEMU [13], [14] to perform fault injection campaigns. This approach is four times faster than simulation-based techniques [15], and unlike simulation-based or formal method-based fault injections techniques, the size of the evaluated circuit has no major impact on the fault injection campaign timing performances. However, configuring an emulation environment can be complex and time-consuming. Achieving an accurate representation of the target system may require detailed configuration and parameter tuning. The accuracy of emulation is contingent on the quality of the models used to replicate the target hardware. If the models are inaccurate or incomplete, the results of fault injections may not precisely reflect actual behaviour.

Formal methods provide an advantage with mathematical proofs, ensuring a rigorous verification of the system's behaviour during fault injection experiments. Formal methods approaches such as [5] allow the analysis of a circuit design in order to detect sensitive logic or sequential hardware elements. [6], [7] and [8] present formal verification methods to analyse the behaviour of HDL implementation. However, this type of tool usually suffers from restrictions limiting its actual usage on a complete processor. Conventional formal approaches encounter scalability challenges due to limitations in verification techniques. In particular, the circuit structure it can analyse is usually limited.

Fault Injections simulations can be performed at processor instructions level. Authors of [9] explore the impact of fault injection attacks on software security. They evaluate four open-source fault simulators, comparing their techniques and suggest enhancing them with AI methods inspired by advances in cryptographic fault simulation. [10] is an open-source deterministic fault attack simulator prototype utilising the Unicorn Framework and Capstone disassembler. [11] introduces VerFI, a gate-level granularity fault simulator for hardware implementations. For instance, it has been used to spot an implementation mistake in ParTI [20]. However, this tool has been developed to check if implemented countermeasures can really protect against fault injection on cryptographic implementations, but it cannot evaluate components such as registers or memories. In this paper, we focus on CABA simulations, which provides a controlled virtual environment for injecting faults. There are several solutions of simulations in an HDL simulator like Questasim, Vivado, etc. *Behavioural* simulation is used to detect functional issues and ensuring that the design behaves as expected. *Post-synthesis* simulation verifies that the synthesised netlist matches the expected functionality. *Timed* simulation is used to ensure that the design meets timing requirements and can operate at the specified clock frequency. And finally, *post-implementation* simulations are used to

verify that the implemented design meets all requirements and constraints, including those related to the physical layout on the target. Simulation-based fault injection offers the advantage of enabling designers to test their system throughout the design cycle, providing valuable insights and uncovering potential vulnerabilities early in the development process. However, a limitation lies in the potential lack of absolute fidelity to actual conditions, as simulations might not perfectly replicate all hardware intricacies, introducing a slight risk of overlooking certain faults that could manifest in the actual hardware.

Table 4.1 shows a comparison between these four methods for vulnerability assessment when considering FIA regarding six metrics. These metrics are the financial cost of setting up the fault injection campaign, the control over fault scenarios (how configurable are the scenarios), scalability which refers to the method capacity to be applied to systems of different sizes or complexities, speed of execution of the campaign, realism of the fault injection campaign and the level of required expertise. Table 4.1 shows that no method is completely optimal. Each method has its own advantages and disadvantages and must be chosen by the designer according to the requirements and the available financial and human resources. Indeed, setting up an actual fault injection campaign requires much more expertise in this domain and also requires costly equipment, whereas setting up a simulation campaign can be easier for a circuit designer familiar with HDL simulation tools such as Questasim. Table 4.1 shows that CABA simulation offers a good compromise to assess the security level of a circuit design. In particular, it provides an efficient solution for investigating security throughout the design cycle, enabling the concept of "Security by Design".

4.2 FISSA

This section presents our open-source tool, FISSA, available on GitHub [21] under the CeCILL-B licence.

4.2.1 Main software architecture

FISSA is designed to help circuit designers to analyse, throughout the design cycle, the sensitivity to FIA of the developed circuit. Figure 4.1 presents the software architecture of FISSA. It consists of three different modules: *TCL generator*, *Fault Injection Simulator* and *Analyser*. The first and third modules correspond to a set of Python classes.

The TCL generator, detailed in Section 4.2.3, relies on a configuration file and a target file to create a set of parameterised TCL scripts. These scripts are tailored based on the provided configuration file and are used to drive the fault injection simulation campaign.

Fault Injection Simulator, detailed in Section 4.2.4, performs the fault injection simulation campaign based on inputs files from *TCL generator* for a circuit design described through HDL files and memory initialisation files. For that purpose it relies on an existing HDL simulator such as Questasim [22], Verilator [23], or Vivado [24] to simulate the design according to the TCL script and generates JSON files to log each simulation.

The Analyser, detailed in Section 4.2.5, evaluates the outcomes of the simulations and generates a set of files that allows the designers to examine fault injection effects on their designs through various information.

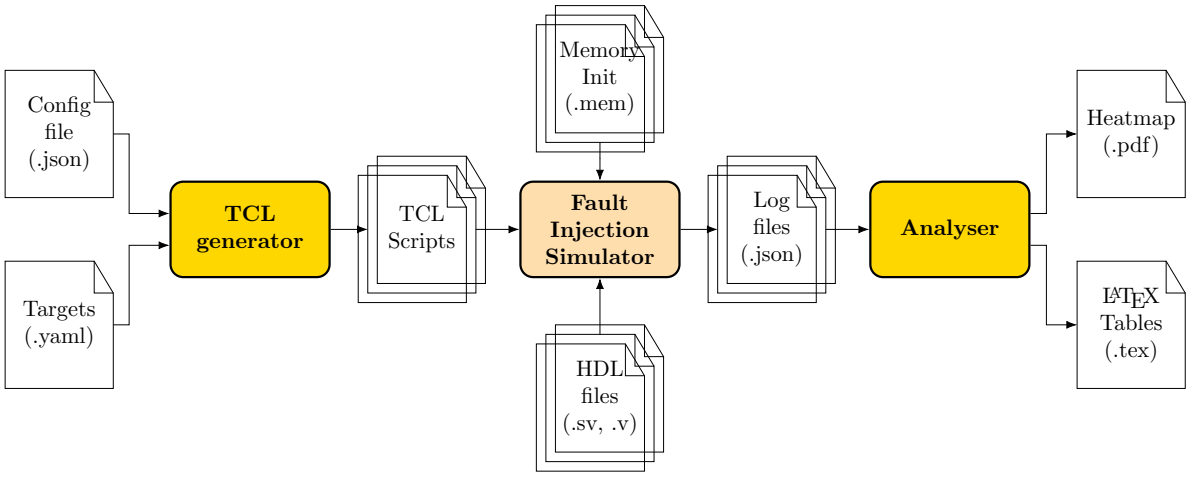

Figure 4.1: Software architecture of FISSA

Algorithm 1 shows a representation of a fault injection campaign. The algorithm requires a set of targets (i.e. hardware elements in which a fault should be injected), the fault model and the considered injection window(s) which identifies the period(s), in number of clock cycles, in which fault injections are performed. Then, it runs a first simulation with no fault injected, which is used as a reference for comparison with the following simulations to determine end-of-simulation statuses. Then, for each target, each fault model and for each clock cycle within the injection window, the corresponding simulation is executed, and the corresponding logs are stored in a dedicated file.

Customising end-of-simulation statuses allows for adaptation to the specific requirements of each design assessment. To configure these statuses, adjustments need to be made either directly in FISSA's code or the HDL code. This process may involve evaluating factors such as:

- hardware element content (signals, registers, ...),
- simulation time (e.g. the simulation exceeds a reference number of clock cycles),
- simulation's end (e.g. an assert statement introduced in the HDL code is reached)

Algorithm 1 Simulated FIA campaign pseudo-code

Require: $targets \leftarrow list(targets)$
Require: $faults \leftarrow list(fault\_model)$
Require: $windows \leftarrow list(injection\_windows)$
1: $ref\_sims = simulate()$
2: **for** $target \in targets$ **do**
3: **for** $fault \in faults$ **do**
4: **for** $cycle \in windows$ **do**
5: $logs = simulate(target, fault, cycle)$
6: **end for**
7: **end for**
8: **end for**

4.2.2 Supported fault models

A set of fault models has already been integrated into FISSA for different needs. For a given fault injection campaign, the relevant fault model is defined in the input configuration file and is applied to targets during the simulation phase. Currently, supported fault models are:

- target set to 0/1: for each cycle of the injection window and for each target, we set them individually to 0 or 1, in turn exhaustively ($nbSimulations = nbCycles * nbTargets$),
- single bit-flip in one target at a given clock cycle: for each cycle of the injection window, we do a bit-flip for each bit of every targets exhaustively ($nbSimulations = nbCycles * nbBits$),
- single bit-flip in two targets at a given clock cycle: we take one cycle and a couple of targets' bits (it can be the same target at two different bits) and we bit-flip these two bits ($nbSimulations = nbCycles * C_2^k$; with k, the total number of bits in the attacked system),
- single bit-flip in two targets at two different clock cycles: we take two different cycles and a couple of targets' bits (it can be the same target at two different bits) and we bit-flip these two bits ($nbSimulations = C_2^{nbCycles} * C_2^k$; with k, the total number of bits in the attacked system),
- exhaustive multi-bits faults in one target at a given clock cycle: we take one cycle and one target and we try exhaustively each combinations of bits (for example for a 2 bits target, it would be: 00, 01, 10, 11) and we set the target at each value ($nbSimulations = nbCycles * 2^{targetSize1}$). It is worth nothing that for this fault model, we only take targets between 1 and 16 bits to avoid very big numbers of simulations as 2^{32} would be too long to simulate exhaustively,
- exhaustive multi-bits faults in two targets at a given clock cycle: we take one cycle and two targets and we try exhaustively each combinations of bits (for example for a 2 bits target, it would be: 00, 01, 10, 11) for each target and we set them to each value ($nbSimulations = nbCycles * 2^{targetSize1} * 2^{targetSize2}$). It is worth nothing that for this fault model, we only take targets between 1 and 10 bits to avoid very big numbers of simulations as 2^{32} would be too long to simulate exhaustively.

4.2.3 TCL Generator

The *TCL Generator* is used to generate the set of TCL script files which drive the *fault injection simulator*. This module requires two input files. Figure 4.2 details the *TCL Generator*. Each blue box represents a python class used to generate the set of output TCL scripts. The *initialisation* class gets inputs from a configuration file. This JSON-formatted file includes various parameters such as the targeted HDL simulator, the considered fault model and the injection window(s). Furthermore, it encompasses parameters such as the clock period (in ns) of the HDL design and the maximum number of simulated clock cycles used to stop the simulation in case of divergence due to the injected fault. Moreover, one extra parameter defines the quantity of simulations per TCL file, allowing a simulation parallelism degree. Listing 4.1 shows an example of a configuration file used for our fault injection campaigns.

The *Targets* file contains, in YAML format, the list of the circuit elements (e.g. registers or logic gates) that need to be targeted during the fault injection campaign. For each target, its HDL path and

Listing 4.1: Example of a FISSA configuration file

```
{
    "name_simulator": "modelsim",
    "path_tcl_generation": "PATH/",
    "path_files_sim": "PATH/simu_files/",
    "path_generated_sim": "PATH/simu_files/generated_simulations/",
    "path_results_sim": "PATH/simu_files/results_simulations/",
    "path_simulation": [ "PATH_SIMU/"],
    "prot": "wop",
    "version": 1,
    "name_reg_file_ext_wo_protect": "/faulted-reg.yaml",
    "application": ["buffer_overflow", "secretFunction", "propagationTagV2"],
    "name_results": {
        "buffer_overflow": "Buffer Overflow",
        "secretFunction": "WU-FTPd",
        "propagationTagV2": "Compare/Compute"
    },
    "threat_model": [
        "single_bitflip_spatial"
    ],
    "multi_fault_injection": 2,
    "avoid_register": [],
    "avoid_log_registers": [],
    "log_registers": [],
    "injection_window": {
        "buffer_overflow": [
            [137140, 137380]
        ],
        "secretFunction": [
            [2099100, 2099420]
        ],
        "propagationTagV2": [
            [33300, 33460]
        ]
    },
    "cycle_ref": 100,
    "cpu_period": 40,
    "batch_sim": {
        "buffer_overflow": 2000,
        "secretFunction": 2000,
        "propagationTagV2": 2000
    },
    "multi_res_files": {
        "buffer_overflow": 8,
        "secretFunction": 8,
        "propagationTagV2": 8
    }
}
```

bit-width are specified. *TCL Script Generator* class gets the configuration parameters from *Initialisation* class, reads the *Targets'* file and calls three others classes. The first one, *Basic Code Generator*, undertakes the fundamental generation of TCL code for initialising a simulation, running a simulation, and ending a simulation. The second one, *Fault Generator*, produces the TCL code related to fault injection. The *TCL Script Generator* provides specific parameters to the *Fault Generator* to produce code for a designated set of targets and a specified set of clock cycles for fault injection. The third one, *Log Generator*, produces the TCL code to produce logs after each simulation. Logs comprise the simulation's ID, fault model, faulted targets, injection clock cycle(s), end-of-simulation status, values for all targets, and the end-of-simulation clock cycle. This data constitutes the automated aspect of logging. Finally, the *TCL Script Generator* outputs a set of TCL files, each one correspond to a batch of simulations. This allows the user to perform a per batch results analysis. It is worth noting that each batch starts with a reference simulation which means a simulation without any fault injected. It allows to have results for comparison after when a fault occured and determine what happened due to the injected fault. Additionally, it generates a target file utilised by TCL scripts to obtain a simplified target list (refer to Subsection 4.2.4), as the simulation log requires a list of targets without their sizes.

Algorithm 2 depicts a fault injection simulation pseudo-code, showcasing requirements, and each state with essential parameters. Additionally, the corresponding Python class from Figure 4.2 is added for each line. Line 5 in Algorithm 1 corresponds to Algorithm 2. This algorithm is executed multiple times with different inputs to build a TCL script.

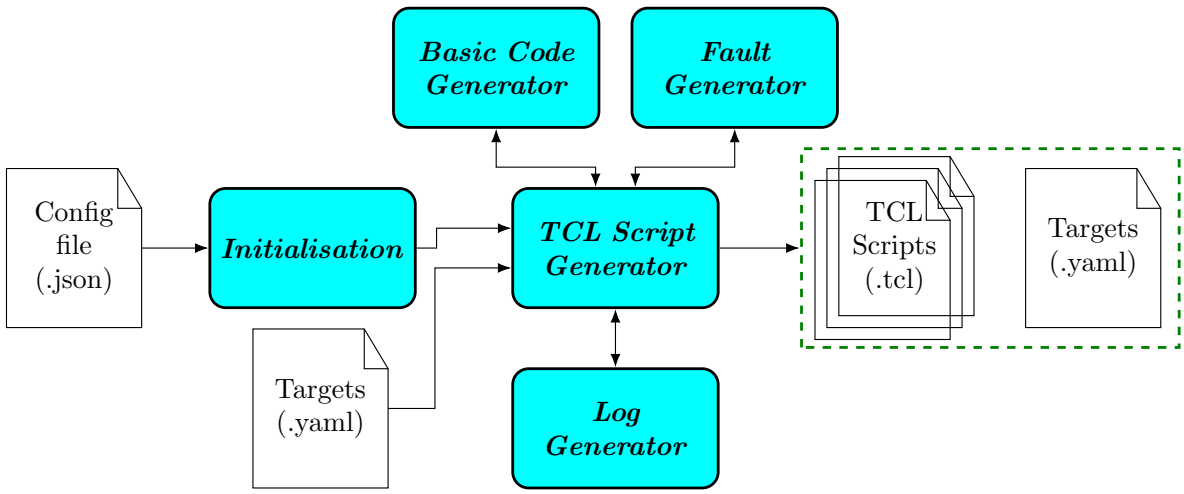

Figure 4.2: Software architecture of the TCL Generator module

Algorithm 2 FIA simulation pseudo-code

Require: $target$
Require: $cycle$
Require: $fault\_model$
1: $tcl\_script = init\_sim(fault\_model, cycle, target)$ // generated by Basic Code Generator
2: $tcl\_script+ = inject\_fault(fault\_model)$ // generated by Fault Generator
3: $tcl\_script+ = run\_sim()$ // generated by Basic Code Generator
4: $tcl\_script+ = log\_sim(fault\_model)$ // generated by Log Generator
5: $tcl\_script+ = end\_sim()$ // generated by Basic Code Generator
6: $tcl\_file.write(tcl\_script)$ // append and write the simulation data inside the TCL file

4.2.4 Fault Injection Simulator

The *Fault Injection Simulator* mainly relies on an existing HDL simulator to perform simulations by executing the TCL scripts produced by the *TCL generator*. The log files, in JSON format, are generated by the TCL script for each simulation. This file encompasses data such as the current simulation number, the executed clock cycle count, the values of the targets' file, the targets faulted, the fault model and the end-of-simulation status.

Listing 4.2 shows a simplified example of an output file from a simulation. Many lines are omitted to simplify the text and its comprehension. In this example, we have the result of the first simulation of the campaign. The fault model is a single bit-flip in one target at a given clock cycle, and the target, which is a register in this case, `pc_id_o_tag`, has a size of one bit. We attack it at the period time of 137,140 ns. The omitted lines, at line 7, include all registers from the register file, all register file tags, and all registers from the target list. The last line, line 14, shows that this simulation ended with a status equal to 3 (i.e., exception delayed from the reference simulation).

It is worth noting that the set of calls to the generated TCL scripts has to be integrated into the designer's existing design flow, allowing the design compilation, initialisation, and management of input stimuli. The use of TCL scripts simplifies such an integration. Once all the fault injection simulations have

been performed, the log files can be sent to the *Analyser* which, is described in the following subsection.

Listing 4.2: Extract of an example of a FISSA output log JSON file

```
"simulation_1": {
    "cycle_ref": 100,
    "cycle_ending": 4,
    "TPR": "32'h0000a8a2",
    "TCR": "32'h00341800",
    "rf1": "32'h000006fc",
    (...)
    "faulted_register": "/tb/top_i/core_region_i/RISCV_CORE/if_stage_i/pc_id_o_tag",
    "size_faulted_register": 1,
    "threat": "bitflip",
    "bit_flipped": 0,
    "cycle_attacked": "137140 ns",
    "simulation_end_time": "137300 ns",
    "status_end": 3
}
```

4.2.5 Analyser

The *Analyser* reads all log files and generates a set of LaTeX tables (*.tex* files) and/or sensitivity heatmaps (in PDF format) according to the fault models, allowing the user to identify the sensitive hardware elements in the circuit design. The generated tables can be customised through modification in the *Analyser* Python code. The current configuration captures and counts the diverse end-of-simulation status. Heatmaps are generated for multi-target fault models. For instance, when considering a 2 faults scenario disturbing two hardware elements, a 2-dimension heatmap allows the user to identify sensitive couples of hardware elements leading to a potential vulnerability. Their configuration can be adapted by modifying the *Analyser* Python code. Heatmaps generation is based on *Seaborn* [25] which relies on *Matplotlib* [26]. This library provides a high-level interface for drawing attractive and informative statistical graphics and save them in different formats like PDF, PNG, etc. In the current configuration, heatmaps highlight the targets leading to a specific end-of-simulation status (e.g. a status identified by the designer as a successful attack). Once the results have been generated, they can easily be inserted into a vulnerability assessment report.

4.2.6 Extending FISSA

In order to extend FISSA for integrating an additional fault model, some modifications to the *TCL Script Generator*, the *Basic Code Generator*, the *Fault Generator* and *Log Generator* modules are necessary. It requires the extension of the *init_sim*, *inject_fault* and *log_sim* functions presented in Algorithm 2 to implement the new fault model from initialisation to logging. For instance, these extensions should define the targets for each simulation, the impact of the injections (set to 0/1, bit-flip, random, etc) and the set of data to be logged for this fault model. The *Log Generator* automates the extraction of specific segments from the ongoing simulation. However, it is customisable, enabling the modification of logged elements, such as incorporating memory content or a list of signals.

Analyser can be extended to produce additional LaTeX tables, heatmaps or any other way of results visualisation. This can be achieved by either modifying the existing methods or by developing new ones.

An integral aspect of expanding FISSA involves adjusting functions depending on the used HDL simulator. Despite the definition of the TCL language, specific commands vary between simulators.

4.3 Example application

4.4 Discussion and Perspectives

4.4.1 Discussion

In this section, we will discuss about this proposed tool and draw some perspectives for the long-term development. In terms of execution time, we did in total around 24,000,000 simulations for approximatively 3 seconds for each simulation in average spanning from initialisation to data recording. The execution time is contingent upon various parameters, including the design's size, the specific simulation case, and the number of targets involve. For example, as we have 3 different use cases, it goes from an average of 0.4 second to 5.8 seconds per simulation. In emulation campaigns, FPGA-based fault emulation is four times faster than simulation-based techniques, as noted in paper [15]. Actual FIAs are faster than simulations, taking about 0.35 seconds per injection in our tests, relying on the ChipWhisperer-lite platform for clock glitching injection. While simulations may be slower, they offer the benefit of not requiring an FPGA prototype or the final circuit. Furthermore, it allows integrating vulnerability assessment in the first stages of the development flow and provides a rich set of information for the designer in order to understand sources of vulnerabilities in his design.

4.4.2 Perspectives

As a perspective, we plan to extend FISSA to support new fault models and HDL simulators such as Vivado or Verilator. Additionally, we intend to enhance integration into the design workflow by adding more automatisation. This may include the management of HDL sources compilation, design's input stimuli or the development of a graphical user interface to improve the overall user experience.

4.5 Summary

In this chapter, we presented FISSA (Fault Injection Simulation for Security Assessment), our advanced and versatile open-source tool designed to automate fault injection campaigns. FISSA is engineered to seamlessly integrate with renowned HDL simulators, such as Questasim. It facilitates the execution of simulations by generating TCL scripts and produces comprehensive JSON log files for subsequent security analysis.

FISSA empowers designers to evaluate their designs during the conceptual phase by allowing them to select specific assessment parameters, including the fault model and target components, tailored to their unique requirements. The insights gained from the results generated by this tool enable designers to enhance the security of their designs, thus adhering to the principles of *Security by Design*.

Chapter 5

Countermeasures Implementations

Contents

5.1 Countermeasure 1: Simple Parity

5.2 Countermeasure 2: Hamming Code

5.2.1 Implementation 1: Optimisation of redundancy bits

5.2.2 Implementation 2: Protection by pipeline stage

5.2.3 Implementation 3: Protection of all registers individually

5.2.4 Implementation 4: Protection of all registers individually with CSRs slicing

5.2.5 Implementation 5: Smart protection by pipeline stage

5.3 Countermeasure 3: Hamming Code - SECDED

5.3.1 Implementation 1: Optimisation of redundancy bits

5.3.2 Implementation 2: Protection by pipeline stage

5.3.3 Implementation 3: Protection of all registers individually

5.3.4 Implementation 4: Protection of all registers individually with CSRs slicing

5.3.5 Implementation 5: Smart protection by pipeline stage

5.4 Summary

Chapter 6

Experimental setup and results

Contents

6.1 Experimental setup

6.2 Experimental results

Chapter 7

Conclusion

The only truly secure system is one that is powered off, cast in a block of concrete and sealed in a lead-lined room with armed guards - and even then I have my doubts.

Gene Spafford

Contents

7.1 Synthesis

7.2 Perspectives

BIBLIOGRAPHY

[1] C. Palmiero, G. Di Guglielmo, L. Lavagno, and L. P. Carloni, "Design and Implementation of a Dynamic Information Flow Tracking Architecture to Secure a RISC-V Core for IoT Applications", *in High Performance Extreme Computing*, 2018. DOI: 10.1109/HPEC.2018.8547578.

[2] C. Palmiero, G. Di Guglielmo, L. Lavagno, and L. P. Carloni. "A Hardware Dynamic Information Flow Tracking Architecture for Low-level Security on a RISC-V Core". (2018), [Online]. Available: https://github.com/sld-columbia/riscv-dift.

[3] S. Loosemore, R. M. Stallman, R. McGrath, A. Oram, and U. Drepper. "The GNU C Library Reference Manual". (2023), [Online]. Available: https://www.gnu.org/s/libc/manual/pdf/libc.pdf.

[4] W. Pensec, V. Lapôtre, and G. Gogniat, "Another Break in the Wall: Harnessing Fault Injection Attacks to Penetrate Software Fortresses", *in Proceedings of the First International Workshop on Security and Privacy of Sensing Systems*, ser. SensorsS&P, Istanbul, Turkiye: Association for Computing Machinery, 2023, pp. 8–14. DOI: 10.1145/3628356.3630116.

[5] J. Richter-Brockmann, A. Rezaei Shahmirzadi, P. Sasdrich, A. Moradi, and T. Güneysu, "FIVER – Robust Verification of Countermeasures against Fault Injections", *IACR Transactions on Cryptographic Hardware and Embedded Systems*, 2021. DOI: 10.46586/tches.v2021.i4.447-473.

[6] V. Arribas, S. Nikova, and V. Rijmen, "VerMI: Verification Tool for Masked Implementations", *in 25th IEEE International Conference on Electronics, Circuits and Systems (ICECS)*, 2018. DOI: 10.1109/ICECS.2018.8617841.

[7] G. Barthe, S. Belaïd, G. Cassiers, P.-A. Fouque, B. Grégoire, and F.-X. Standaert, "maskVerif: Automated Verification of Higher-Order Masking in Presence of Physical Defaults", *in Computer Security – ESORICS 2019: 24th European Symposium on Research in Computer Security, Proceedings, Part I*, 2019. DOI: 10.1007/978-3-030-29959-0_15.

[8] S. Tollec, V. Hadžić, P. Nasahl, *et al.*, "Fault-resistant partitioning of secure cpus for system co-verification against faults", 2024. [Online]. Available: https://eprint.iacr.org/2024/247.

[9] A. Adhikary and I. Buhan, "SoK: Assisted Fault Simulation", *in Applied Cryptography and Network Security Workshops*, Springer Nature Switzerland, 2023. DOI: 10.1007/978-3-031-41181-6_10.

[10] Riscure, *FiSim: An open-source deterministic Fault Attack Simulator Prototype*. [Online]. Available: https://github.com/Riscure/FiSim.

[11] V. Arribas, F. Wegener, A. Moradi, and S. Nikova, "Cryptographic Fault Diagnosis using VerFI", *in IEEE International Symposium on Hardware Oriented Security and Trust (HOST)*, 2020. DOI: 10.1109/HOST45689.2020.9300264.

[12] G. Canivet, P. Maistri, R. Leveugle, J. Clédière, F. Valette, and M. Renaudin, "Glitch and laser fault attacks onto a secure AES implementation on a SRAM-based FPGA", *Journal of cryptology*, 2011. DOI: 10.1007/s00145-010-9083-9.

[13] F. Hauschild, K. Garb, L. Auer, B. Selmke, and J. Obermaier, "ARCHIE: A QEMU-Based Framework for Architecture-Independent Evaluation of Faults", *in Workshop on Fault Detection and Tolerance in Cryptography (FDTC)*, 2021. DOI: 10.1109/FDTC53659.2021.00013.

[14] Y. B. Bekele, D. B. Limbrick, and J. C. Kelly, "A Survey of QEMU-Based Fault Injection Tools & Techniques for Emulating Physical Faults", *IEEE Access*, 2023. DOI: 10.1109/ACCESS.2023.3287503.

[15] R. Nyberg, J. Nolles, J. Heyszl, D. Rabe, and G. Sigl, "Closing the Gap between Speed and Configurability of Multi-bit Fault Emulation Environments for Security and Safety-Critical Designs", *in 17th Euromicro Conference on Digital System Design*, 2014. DOI: 10.1109/DSD.2014.39.

[16] H. Bar-El, H. Choukri, D. Naccache, M. Tunstall, and C. Whelan, "The Sorcerer's Apprentice Guide to Fault Attacks", *Proceedings of the IEEE*, 2006. DOI: 10.1109/JPROC.2005.862424.

[17] C. Bozzato, R. Focardi, and F. Palmarini, "Shaping the Glitch: Optimizing Voltage Fault Injection Attacks", *IACR Transactions on Cryptographic Hardware and Embedded Systems*, 2019. DOI: 10.13154/tches.v2019.i2.199-224.

[18] P. Grandamme, L. Bossuet, and J.-M. Dutertre, "X-Ray Fault Injection in Non-Volatile Memories on Power OFF Devices", *in 2023 IEEE Physical Assurance and Inspection of Electronics (PAINE)*, 2023. DOI: 10.1109/PAINE58317.2023.10318018.

[19] B. Colombier, P. Grandamme, J. Vernay, *et al.*, "Multi-Spot Laser Fault Injection Setup: New Possibilities for Fault Injection Attacks", *in Smart Card Research and Advanced Applications*, V. Grosso and T. Pöppelmann, Eds., 2022. DOI: 10.1007/978-3-030-97348-3_9.

[20] T. Schneider, A. Moradi, and T. Güneysu, "ParTI–towards combined hardware countermeasures against side-channel and fault-injection attacks", *in Advances in Cryptology–CRYPTO: 36th Annual International Cryptology Conference, Proceedings, Part II 36*, 2016. DOI: 10.1007/978-3-662-53008-5_11.

[21] W. Pensec, *FISSA: Fault Injection Simulation for Security Assessment*. [Online]. Available: https://github.com/WilliamPsc/FISSA.

[22] Siemens, *QuestaSim*. [Online]. Available: https://eda.sw.siemens.com/en-US/ic/questa/simulation/advanced-simulator/.

[23] Verilator, *Verilator*. [Online]. Available: https://github.com/verilator/verilator.

[24] Xilinx, *Vivado Design Suite*. [Online]. Available: https://www.xilinx.com/products/design-tools/vivado.html.

[25] M. L. Waskom, "Seaborn: statistical data visualization", *Journal of Open Source Software*, 2021. DOI: 10.21105/joss.03021.

[26] J. D. Hunter, "Matplotlib: A 2D graphics environment", *Computing in Science & Engineering*, 2007. DOI: 10.5281/zenodo.7697899.

Titre : titre (en français).....

Mot clés : de 3 à 6 mots clefs

Résumé : Eius populus ab incunabulis primis ad usque pueritiae tempus extremum, quod annis circumcluditur fere trecentis, circummurana pertulit bella, deinde aetatem ingressus adultam post multiplices bellorum aerumnas Alpes transcendit et fretum, in iuvenem erectus et virum ex omni plaga quam orbis ambit inmensus, reportavit laureas et triumphos, iamque vergens in senium et nomine solo aliquotiens vincens ad tranquilliora vitae discessit. Hoc inmaturo interitu ipse quoque sui pertaesus excessit e vita aetatis nono anno atque vicensimo cum quadriennio imperasset. natus apud Tuscos in Massa Veternensi, patre Constantio Constantini fratre imperatoris, matreque Galla. Thalassius vero ea tempestate praefectus praetorio praesens ipse quoque adrogantis ingenii, considerans incitationem eius ad multorum augeri discrimina, non maturitate vel consiliis mitigabat, ut aliquotiens celsae potestates iras principum molliverunt, sed adversando iurgandoque cum parum congrueret, eum ad rabiem potius evibrabat, Augustum actus eius exaggerando creberrime docens, idque, incertum qua mente, ne lateret adfectans. quibus mox Caesar acrius efferatus, velut contumaciae quoddam vexillum altius erigens, sine respectu salutis alienae vel suae ad vertenda opposita instar rapidi fluminis irrevocabili impetu ferebatur. Hae duae provinciae bello quondam piratico catervis mixtae praedonum.

Title: titre (en anglais).....

Keywords: de 3 à 6 mots clefs

Abstract: Eius populus ab incunabulis primis ad usque pueritiae tempus extremum, quod annis circumcluditur fere trecentis, circummurana pertulit bella, deinde aetatem ingressus adultam post multiplices bellorum aerumnas Alpes transcendit et fretum, in iuvenem erectus et virum ex omni plaga quam orbis ambit inmensus, reportavit laureas et triumphos, iamque vergens in senium et nomine solo aliquotiens vincens ad tranquilliora vitae discessit. Hoc inmaturo interitu ipse quoque sui pertaesus excessit e vita aetatis nono anno atque vicensimo cum quadriennio imperasset. natus apud Tuscos in Massa Veternensi, patre Constantio Constantini fratre imperatoris, matreque Galla. Thalassius vero ea tempestate praefectus praetorio praesens ipse quoque adrogantis ingenii, considerans incitationem eius ad multorum augeri discrimina, non maturitate vel consiliis mitigabat, ut aliquotiens celsae potestates iras principum molliverunt, sed adversando iurgandoque cum parum congrueret, eum ad rabiem potius evibrabat, Augustum actus eius exaggerando creberrime docens, idque, incertum qua mente, ne lateret adfectans. quibus mox Caesar acrius efferatus, velut contumaciae quoddam vexillum altius erigens, sine respectu salutis alienae vel suae ad vertenda opposita instar rapidi fluminis irrevocabili impetu ferebatur. Hae duae provinciae bello quondam piratico catervis mixtae praedonum.